BNL-225295-2024-TECH
EIC-ADD-TN-086

Recent Beam Stability Analysis for the EIC

A. Blednykh

December 2023

Electron-Ion Collider

Brookhaven National Laboratory

U.S. Department of Energy

USDOE Office of Science (SC), Nuclear Physics (NP)

DISCLAIMER

Recent Beam Stability Analysis for the EIC

M. Blaskiewicz*, A. Blednykh, X. Gu, C. Montag, I. Pinayev,
B. Podobedov, V. Ptitsyn, V. Ranjbar
Brookhaven National Laboratory Upton, New York 11973, USA
Themis Mastoridis,
California Polytechnic State University, San Luis Obispo, USA

December 2023

1 Introduction

This document summarizes work done in WBS 6.02.02 during FY23. Additional details can be found in the EIC overview paper presented at IPAC'23 [1], and the references therein. Progress has been made in the ESR and HSR lattice design, dynamic aperture optimization, and the RCS lattice design. The impedance and Collective effects are progressing and include the impedance optimization process of the vacuum systems for RCS, HSR, and ESR; collective effects studies; collective effects and beam-beam interaction; coupled bunch instabilities and the crab cavities; low-level RF feedback system design and beam-ion instability. The reversed phasing RF system has been numerically studied for the ESR to mitigate Robinson instability and demonstrate reliable stable beam operation. Various codes, including C++, SPACE [2], ELEGANT [3], and Mbtrack2 [4] have been employed to benchmark the results. The simulation of HSR bunch splitting with beam loading has been performed at 275 GeV energy. The evaluation of Beam Position Monitors aimed to validate their expected performance, with the primary objective being to verify their accuracy. Calculations of Electron Polarization in the ESR, RCS, and HSR are showing good progress. In the RCS, preliminary studies indicate excellent polarization transmission over intrinsic spin resonances, achieving over 90% transmission with improved performance compared to the previous lattice. Preliminary simulations in the ESR indicate encouraging results in minimizing depolarization and improving equilibrium polarization.

*blaskiewicz@bnl.gov

2 ESR Lattice Design, sufficient for arc vacuum system design

The ESR lattice [5] has reached nearly sufficient maturity to allow the engineering design of the arc vacuum system components. It is unlikely that the remaining ESR lattice work will have any impact on the arcs since it is being performed in the IR6 interaction region. This work is expected to be finished by the end of February 2024. The present ESR lattice provides interaction regions, in IR6 and IR8. For studies with only a single interaction region, the β^* values IR8 have been raised substantially to reduce the chromatic contribution of IR8 to values similar to other straight sections. In a future lattice release, an option with a simple cross-over between ESR and HSR will be provided.

3 ESR Dynamic Aperture

Dynamic aperture optimization has been performed for several lattice configurations [6, 7]. The minimum goal of 10σ has been achieved at 5, 10, and 18 GeV, with two colliding interaction regions. Multipole errors in the quadrupoles and sextupoles are taken from the measured APS data, while multipole errors in the dipoles are based on a preliminary error analysis by the magnet design group. These studies will be refined as the dipole design and associated error analysis matures.

4 HSR Lattice Design

The HSR lattice design has been steadily progressing, with the focus on a lattice with two colliding interaction regions, in IR6 and IR8. The reason for this design choice is the fact that we need to ensure that the EIC can support two interaction regions with their low β^* values and resulting large chromaticity contributions. For studies with a single interaction region, the interaction region in IR8 has been detuned in the sense that the β^* values have been raised substantially to the point where the chromatic contribution of IR8 is similar to that of other straight sections. In a future lattice release, a version with a simple cross-over between ESR and HSR in IR8 will be provided

5 HSR Dynamic Aperture

Dynamic aperture studies in the HSR have been performed and are still ongoing. With a single colliding interaction region in IR6, and using preliminary assumptions for the IR magnet multipoles, the dynamic aperture is comparable to present RHIC (same simulation code, same number of turns, etc.). With two interaction regions the dynamic aperture still falls short of the minimum goal when the actual, preliminary IR8 design with its secondary focus is included.

6 RCS Lattice Design

There are several technical questions which we have been studying that impact the development of the RCS lattice design. These include the following:

1. The effect of ambient fields on the 400 MeV beam.
2. The large dynamic range of the energy from 400 MeV to 18 GeV (a factor of 45) raises questions about the quality fields for the RCS's magnets at injection.
3. Collective effects for 7 and 28 nC bunches at energies below 2 GeV make achieving beam stability difficult
4. Eddy currents induced due to the interaction between the fields of the magnets and the vacuum chamber will create sextupole and other multipolar fields at injection energies which are relatively large.

The RCS lattice has been maturing well with versions evolving based on obstructions and interference in the tunnel. Modifications have also been made to the straight sections to reduce the β functions to raise the instability threshold (item 3). We have also performed studies to include the effects of octupoles to help maintain stability.

To understand the impact of ambient fields at low energy (item 1) we have embarked on an intensive campaign to measure the ambient field throughout the tunnel as well as during RHIC operations. As well we have also studied the impact of ambient fields on the beam dynamics using both qualitative and direct tracking models using the RCS lattice. The linearity and stability of the fields at low fields have been studied using an RCS dipole test magnet developed during the past year (item 2).

Also during the past year we came to understand the potential impact of the interaction between the magnetic field and the vacuum chamber. This interaction will lead to eddy currents which will create multipole fields (item 4). We have calculated the strength of these fields using both analytical and numerical approaches. We have also investigated approaches to counter the effects of these fields using existing sextupoles and/or the use of wire compensation.

7 RCS Dynamic Aperture

We have performed studies of the RCS dynamic aperture as well as field error tolerance calculations for the L2S1 version of the lattice and these were reported in the IPAC paper [8]. We have also started similar studies for the new low average beta RCS lattice which we plan on calling the L3S1 version. All of these show that we can achieve a maximum $\delta = \pm 1.5\%$.

Finally, there was progress in developing the Energy and RF ramp for the RCS. The development of the RF voltage and phase ramp from injection energy at 400 MeV to 5, 10, and 18 GeV extraction energy requires control of the bunch's longitudinal aspect ratio to avoid both collective instabilities, RF bucket height, and width as well as lattice dynamic aperture limits [9]

8 IR Lattice Design

The IR lattice has been refined in an iterative manner to resolve mechanical interferences. A local decoupling scheme for the hadron beam line has been developed to compensate for the effect of the detector solenoid. However, this scheme relies on rather strong skew quadrupoles that are difficult to integrate into the tight lattice with its many elements and constraints. The current focus lies on modifying this scheme to reduce the skew quadrupole strengths. An orbit correction scheme is being developed but still needs verification by simulating the effect on the synchrotron radiation background in the detector.

9 Transfer Lines

Transfer lines for both electrons and hadrons have been designed. Future modifications may be driven by lattice modifications in the associated accelerator rings, or by a fundamentally different electron injection scheme. During the past year, the design of the transfer line magnets has been investigated.

10 Engineering Support for Accelerator Layout

Engineering support for accelerator layout in the existing tunnel environment is ongoing. Based on "survey" files generated by the MAD-X accelerator design code, individual accelerator components have been modeled and placed into the appropriate locations in a CAD program to identify potential mechanical interferences. These interferences were then reported back to the accelerator design team to guide the required layout modifications.

By the end of CY23, all interferences have been resolved. However, the outer diameter of the ESR spin rotator solenoid cryostats is only based on a "best guess", since no detailed engineering design of these components exists. Based on this estimate, the solenoids stay clear of the tunnel wall by only 1 to 2 inches. It is expected that the tunnel wall location has a similar uncertainty, so efforts are being made to re-design the spin rotator section based on longer, weaker solenoids which would require less material for the return yoke and therefore have a smaller outer diameter. This work is still ongoing.

11 Impedance and Collective Effects

Impedance calculations are continued for the Rapid Cycling Synchrotron (RCS), Electron Storage Ring (ESR), and Hadron Storage Ring (HSR). Single-bunch studies involved the pseudo-Green function simulations for ESR and HSR with a 0.5mm and 4mm bunch length respectively. To benchmark the results, three different electrodynamics codes, CST [10], GdfidL [11], and ECHO 3D [12], were applied. For HSR, analyses included the beam screen with pump slots, polarimeter, Roman pot, hydrogen jet, BPM Cryo Button with bellows, and bellows with pump ports. ECHO 3D results aligned well with GdfidL but showed discrepancies with CST, particularly noticeable in long-range potentials, prompting the need for further convergence studies.

The impedance budget for ESR has been updated based on the vacuum system's design progress. The main focus was on the optimization of the tapered transition attached to the main 591 MHz cavity. Although the chosen tapered transition length (1:6 ratio) has minimal impact on the total impedance budget, the loss factor, and the kick factors. All the studies proved beneficial for cross-code comparisons, identifying discrepancies and ongoing challenges in the wakefield calculations for the vacuum components.

The RCS impedance budget is a work in progress. Numerical simulations have been performed for only a few vacuum components. Since the RCS impedance budget in its inception, we used the ESR total longitudinal and vertical dipole wakefields for the collective effects simulations.

The Strong Hadron Cooler (SHC) ring-based approach is being considered to reduce both vertical and horizontal emittances at the HSR for high energies. Recent work on the backup ring cooler for the Electron-Ion Collider (EIC) at Brookhaven National Laboratory (BNL) prompted the study of Coherent Wiggler Radiation (CWR) impedance and its effect on the microwave instability threshold. The contribution of CWR to the total impedance budget, especially for 16 DWs at the low-energy ring (150 MeV), is significant. The estimated longitudinal microwave instability threshold due to the CWR impedance of 16 DWs is I_{th}=5 mA, which is smaller than the 31 mA single-bunch current specified in the paper by H. Zhao, J. Kewisch, M. Blaskiewicz, and A. Fedotov [13]. All the results have been published in the refereed journal [14].

Beam-induced heating and thermal analysis have been performed for the vacuum components of the Electron Storage Ring (ESR) and the Hadron Storage Ring (HSR). It addresses the impact of beam-induced resistive wall (RW) losses and synchrotron radiation on ESR vacuum chamber components, as well as the specific concerns for HSR components, such as cryo-cooled systems, bellows, polarimeter, and more.

For the ESR, the study focused on components like the Large Angle Bremsstrahlung Monitor (LABM) and their manageability under calculated losses. Meanwhile, for the HSR, critical com-

ponents like the cryo-cooled BPM button assembly, beam screen, abort kicker, and polarimeters are being analyzed. These analyses involve calculating resistive wall losses using the CST code and evaluating synchrotron radiation via SynRad, both integrated into ANSYS for comprehensive thermal distribution assessment.

Detailed investigations into specific components reveal challenges and potential solutions. For instance, the HSR cryo-cooled BPM button assembly faced significant heating due to resistive wall losses and heat conduction from cryogenic cables. Efforts are made to manage these issues through simulations and design modifications. Similarly, the HSR beam screen undergoes design iterations to mitigate resistive wall heating, considering the placement of steel strips and their impact on heating under radial beam offsets.

Collective effects have been studied for the RCS, ESR, and HSR. In the RCS the beam is single-bunch vertically unstable at the injection energy of 400 MeV and after merging four 7 nC bunches into one at 1 GeV. The Transverse Mode Coupling Instability (TMCI) is caused by the small radius of the vacuum chamber, b=16.5 mm, at low energy and due to a high 28 nC charge at 1 GeV. To stabilize the beam, octupoles are being considered for implementation into the lattice to damp coherent instabilities.

For the ESR, the single-bunch instability thresholds, considering the present impedance budget, are above the required single-bunch current of 2.2 mA by a factor of two for the longitudinal microwave instability threshold and by a factor of 4 for the TMCI threshold at zero chromaticity.

The impedance budget for the HSR is only 50 % complete. As a first approach, we have applied the analytical approximation and the experimentally obtained impedance in RHIC. The instability thresholds are above the single-bunch current at different energies: 41 GeV, 100 GeV, and 275 GeV.

The study of collective effects for low-energy cooling in HSR at 24 GeV is in progress. This includes space charge, geometric, and resistive wall impedance, and their effects on beam stability. The task becomes quite challenging due to the low energy and small synchrotron tune.

Collective effects and beam-beam interaction studies for the EIC are ongoing. For transverse stability the beam beam force is an important source of Landau damping. In the past a weak-strong beam beam model was used and stability during the store was achieved. We are now assessing the impact of coherent beam-beam modes driven by the impedance [15]. A simple model with two transverse dimensions that neglects bunch length effects has been developed. Results are summarized in (Fig. 1). This is a plot of the growth rate of the transverse mode as a function of the bare electron tune. The proton tune was set to 0.36. The beam-beam parameter for the electrons is 0.1 and is 0.02 for the proton beam. There is a purely resistive wakefield which creates an electron instability with growth rate $Im(Q) = 0.004$ in the absence of the beam beam force. All three curves assume the same transverse impedance and beam-beam parameters. The green curve

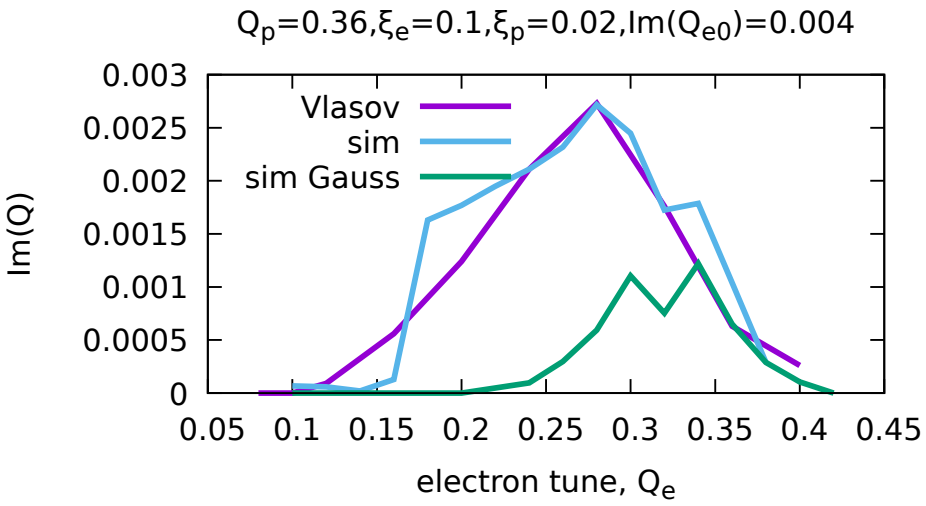

Fig. 1: Instability growth rate versus electron bare tune.

shows tracking results for a Gaussian transverse distribution. The magenta and blue curves show semi-analytic results based on the Vlasov equation and tracking results, respectively. The initial transverse phase space distribution for these curves was

$$F(J_x, J_y) = 6(J_{max} - J_x - J_y)/J_{max}^3. \tag{1}$$

With this distribution it is possible to make significant analytic progress with the Vlasov calculations resulting in faster code. Agreement between the simulations and the Vlasov results are quite good; measuring the growth rate with the simulations is tricky, since the beam always goes nonlinear at large amplitudes. As one can see, there is a significant range of electron tune leading to instability. This theory is adequate to obtain rough results but a more accurate tracking code is under development. BeamBeam3D and TRANFT, developed by Ji Qiang (LBNL) and Michael Blaskiewicz (BNL) respectively have been merged to perform the simulations.

One of the most important coupled bunch instabilities involves the crab cavities [16]. We are designing a feedback system to reduce the apparent impedance of the fundamental crab cavity mode. This work is being done in collaboration with Prof. Themis Mastoridis of CalPoly and his student Trevor George Loe. A paper is in preparation but a short discussion is warranted.

There are two primary parts to this work. The first is to get an accurate model of the impedance

including the effects of feedback and the second is to ascertain the effect of the impedance on the beam.

The feedback model involves well developed tools. First we start with the bare impedance for a transverse mode,

$$Z_{x,ol}(\omega) = \frac{\omega_r R_x}{\omega(1 + iQ_l(\omega_r/\omega - \omega/\omega_r))} \tag{2}$$

where Q_l is the loaded quality factor, R_x is the shunt impedance and ω_r is the cavity fundamental angular frequency. From equation 2 we can see that the resistance will have a peak at $\omega = \omega_r$.

The RF feedback here is modeled simply as a proportional controller with gain G_{fb}, phase ϕ_{fb}, and delay τ_d. The closed-loop impedance then becomes

$$Z_{x,cl}(\omega) = \frac{Z_{x,ol}(\omega)}{1 + G_{fb}e^{-i(\omega\tau_d + \phi_{fb})}Z_{x,ol}(\omega)/R_x} \tag{3}$$

The system performance is limited by the delay. The optimal gain is given by [17],

$$G_{opt} = \frac{Q_L}{\omega_0 \tau_d}$$

For a delay of 320 ns, the resulting optimal gain is ≈2500 for the 197 MHz cavities and ≈1250 for the 394 MHz cavities. These gains lead to approximately 10 dB gain margin.

The OTFB is modeled according to [18] with a gain of 10. It provides an 11-fold decrease in the impedance at the betatron sidebands of each revolution harmonic. The OTFB filter response is given by

$$H_{OTFB}(\Delta\omega) = G_c \frac{(1 - \alpha_c)e^{\pm i2\pi(\nu_b \pm \nu_s)}e^{-i(T_{rev} - \tau_c)\Delta\omega}}{1 - \alpha_c e^{\pm i2\pi(\nu_b \pm \nu_s)}e^{-iT_{rev}\Delta\omega}}$$

where G_c is the OTFB gain, the parameter α_c controls the filter bandwidth around each betatron sideband, ν_b is the betatron tune, ν_s is the synchrotron tune, T_{rev} is the revolution period, $\Delta\omega$ is the angular frequency offset from the crab cavity resonance, and τ_c is the OTFB delay offset. Note that there are four notches between any two revolution harmonics, at $\nu_b + \nu_s$, $\nu_b - \nu_s$, $-\nu_b + \nu_s$, and $-\nu_b - \nu_s$.

The open-loop, closed-loop, and closed-loop impedance with OTFB are overlayed in Figure 2.

The effect of the impedance on the beam is estimated using the Vlasov equation assuming the primary Landau damping comes from octupoles and weak strong beam-beam. The technique employs a generalized Nyquist criterion that has been used for longitudinal instabilities in the past [19]. The idea is to write down the bunched beam transfer function as a matrix equation. Suppose that things vary as $\exp(-i\Omega t + \epsilon t)$ in the beam frame and use the smooth approximation.

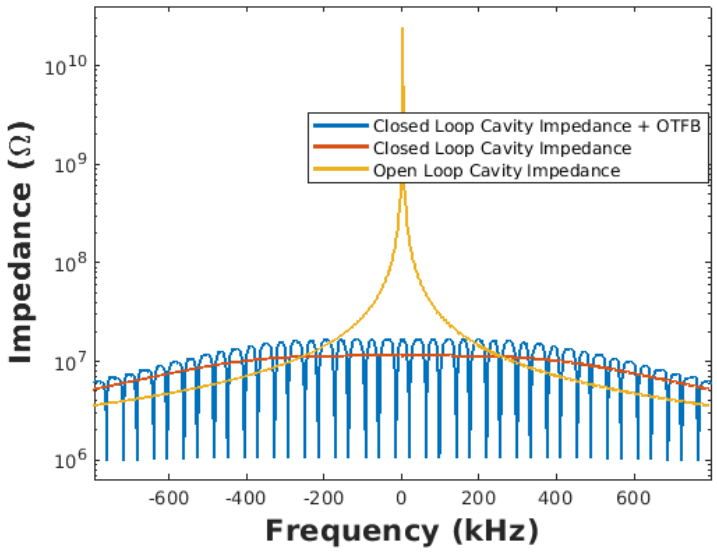

Fig. 2: Crab Cavity transverse impedance.

Then

$$D_k - I_{avg} \sum_{m=-\infty}^{\infty} T_{k,m}(\Omega + i\epsilon) D_m = d_k, \tag{4}$$

where D_k denotes the kth dipole harmonic of the beam, d_k denotes the single particle response to the external drive, I_{avg} is the average beam current and $T_{k,m}$ describes the kick from D_m onto D_k due to collective interactions. The small positive imaginary part ensures causal behavior. For any practical application, the sum needs to be truncated and in matrix notation one has

$$\left(\mathbf{1} - I_{avg}\mathbf{T}(\Omega + i\epsilon)\right)\mathbf{D} = \mathbf{d}. \tag{5}$$

To check stability one plots $Det(1 - I_{avg}\mathbf{T}(\Omega + i\epsilon))$ as a function of Ω on the complex plane. If the contour does not encircle 0 the beam is stable. If the contour does include 0 then one increases ϵ until the contour just passes through 0. That value of ϵ is the growth rate of the most unstable mode. Conversely one can reduce I_{avg} until the contour passes through 0 to get the threshold current. This discussion applies to a single coupled bunch mode and one needs to check other modes to make sure the most unstable mode has been found. The expressions for $T_{k,m}$ are messy and will not be reproduced here. They always employ some approximation but they can be evaluated quickly which allows for optimization. As of now it looks like stability can be assured with reasonable parameters but we are not ready to share details.

12 Beam-Ion Instability Simulations

Beam-ion instability is one of a few collective effects in the ESR which is not driven by the impedance but rather by the residual ions in the vacuum chamber. This instability was predicted [20] to be of concern to the ESR because any coherent motion of the electron beam will be imprinted into ions in the HSR, reducing the luminosity and increasing the detector backgrounds. For accurate instability threshold predictions the simulations must include all relevant physics, such as the beam-beam-induced tune spread, the actual ring lattice, realistic fill pattern, multiple ions species, etc. Some features of the ESR, especially long bunch train, large circumference, and large variation of beta-functions, make these simulations extremely computer intensive and require parallel computations.

The parallel version of Elegant (Pelegant) [3] is especially well-suited for these simulations because its instability modeling was extensively benchmarked against other codes and experimental observations. However, applying this code to the ESR had only become possible recently, after the new "beambeam" element was added to the code, at the EIC team's request. Debugging the implementation and cross-checking the effects of this element against analytical results and other codes took a significant amount of effort, which continued into FY23. In the end, it was confirmed that beam-ion instability simulations with beam-beam provide reliable results.

The bulk of FY23 work included beam-ion instability simulations for the updated vacuum system design, which was partially motivated by the need to suppress the instability. The design has expanded the use of NEG coating which resulted in a factor of 5 reduction in the expected ring-average residual ion pressure, from 5.6 nTorr to 1.12 nTorr.

Simulations with Elegant and other analyses performed to date predict stability for colliding beams. This is very different from the previous vacuum system design where strong instabilities were predicted in simulations. This is illustrated in Fig. (3) , which shows that at 5.6 nTorr and higher ion pressures, there is a strong instability-induced peak centered on the ion oscillation frequency. In contrast, at the pressure corresponding to the new vacuum system design, there is no instability-induced peak, and the residual beam oscillations are statistically indistinguishable from the case without ions.

Future work will include simulations for the latest lattice versions, especially at 5 GeV, as well as further studies of ion-enhanced residual beam oscillations below the instability threshold.

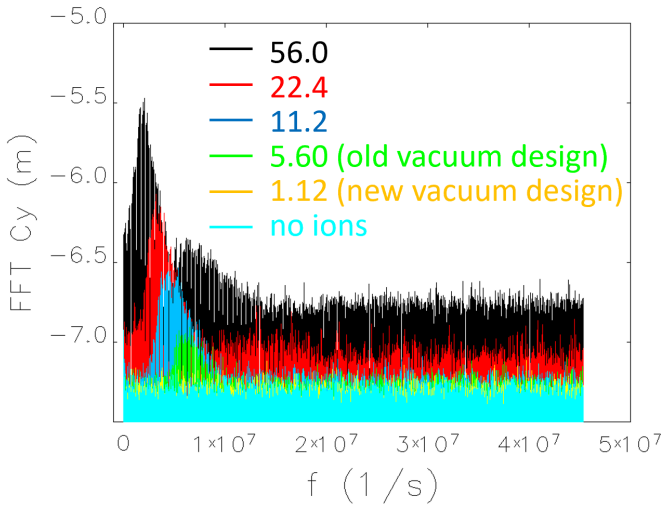

Fig. 3: FFT (log scale) of the vertical beam centroid at the IP at several residual ion pressures for the nominal 1160 bunch fill at 10 GeV. The pressures are marked in the legend in nTorrs.

13 Beam Loading and Beam Gymnastics

13.1 The Reverse Phase Configuration in ESR

We performed a comprehensive study of reversed phasing in the RF system of the Electron Storage Ring (ESR). The ESR of the EIC requires a high-power RF system to compensate losses due to synchrotron radiation and beam-induced wakefields. With the RF voltage of VRF =12 MV at 5 GeV and VRF =24 MV at 10 GeV, the required detuning frequency becomes so large that the beam can be Robinson unstable [21] To avoid this issue, the concept of the reversed phasing RF system is considered as a viable option for stable beam operation. Here we report on the results of ELEGANT and Mbtrack2 simulations for the ESR RF system with reversed phasing using the lattice version of 5.3 at 5 GeV energy. We also present the full beam dynamics results, including energy spread, bunch length, and centroid offset as a function of bunch number in the train. This study provides valuable insights into the feasibility and effectiveness of the reversed phasing RF system for stable beam operation in the ESR at the EIC.

Here we discuss particle tracking simulations for the reversed phasing RF concept using the ELEGANT code [3]. It should be noted that the results simulated by Tianmu Xin, Michael Blaskiewicz, and Gabriele Bassi using C++ and the SPACE [2] codes are in agreement with ELEGANT simulations for different RF system configurations, including 12 focusing and 6 defocusing cavities.

13.1.1 Results from Elegant Code

A ∼10 MW power is required to compensate losses due to synchrotron radiation and beam-induced wakefields in ESR at 2.5 A average current within $M = 1160$ bunches. To reduce the detuning frequency range, the reversed phasing RF system is considered for the EIC project as an option for stable beam operation. It is a well-known concept, when two groups of cavities are set up with the same RF cavity voltage and different synchronous phases. Experimentally, the RF system with the reversed phasing was tested with a beam in KEK B-Factory [22] and no issues during operation were found.

The follwing Equations are discussed for the RF system with focusing and defocusing RF cavities

-Focusing ($\pi/2 \leq \varphi_f \leq \pi$):

$$N_{c,f} V_f \sin\varphi_s + N_{c,d} V_d \sin\varphi_s = V_{RF} \sin\varphi_s \tag{6}$$

-Defocusing ($0 \leq \varphi_d \leq \pi/2$):

$$N_{c,f} V_f \cos\varphi_s - N_{c,d} V_d \cos\varphi_s = V_{RF} \cos\varphi_s, \tag{7}$$

where $N_{c,tot} = N_{c,f} + N_{c,d}$ and $V_c = V_f = V_d$.

The synchronous phase is

$$\sin\varphi_s = \frac{U_0}{N_{c,tot} V_c}, \tag{8}$$

where U_0 is the energy loss per turn, $N_{c,tot}$ is the total number of the RF cavities. After solving the system with two equations, the voltage per cavity V_c is

$$V_c = \sqrt{\frac{V_{RF}^2 - U_0^2}{(N_{c,f} - N_{c,d})^2} + \frac{U_0^2}{N_{c,tot}^2}} \tag{9}$$

The detuning frequency Δf can be found as

$$\Delta f = -f_{RF} \frac{R/Q \cdot I_{av}}{V_c} \sqrt{1 - \frac{U_0^2}{V_{RF}^2}}, \tag{10}$$

where f_{RF} is the RF frequency and I_{av} is the average current.

The main electron beam and the RF system parameters are listed in Table 1 and Table 2. The

beam parameters are related to the 5.3 lattice version. With the updated parameters, the RF system with 10 focusing and 7 defocusing cavities has been simulated. The detune frequencies are much lower than the revolution frequency $f_0 = 78.194kHz$ with a counter phasing scheme. The total number of macroparticles used in ELEGANT is 5k. The results of the particle tracking simulations are presented in Figs. 4, 5, and 6. The bunch length dependence has a parabolic shape (Fig. 4). The bunches at the end of the train have a significantly larger length than the bunches early in the train. The time evolution of the bunch of centroids shows something close to a cotangent behavior along the train (Fig. 5) with their zero offset in the middle of the train. The energy spread $\sigma_\delta(M_i)$ dependence on the number of bunches looks a bit noisy (Fig. 6) due to a less number of macroparticles used during the simulations, but we don't observe an explicit parabolic dependence as in the case of the bunch length. The present simulations have been performed with the RF system only, including the RF cavity impedance. Since the bunch length is varied along the train, it may affect the Robinson threshold with the presence of the beam-induced wakefields and impedances (leading to a tune shift). The minimum bunch length in the middle of the train is $\sigma_s \approx 6mm$. The bunch length spread in the train is $\sim 1mm$.

Energy, E_0	5	GeV
Average Current, I_0	2.5	A
Momentum Compaction, α_c	1.33e-3	
Number of Bunches, M	1160	
Energy Loss per turn, U_0	0.95	MeV
RF Voltage, V_{RF}	10.1	MV
Bunch Length, σ_s	6.8	mm
Energy Spread, σ_δ	5.16e-4	

Table 1: Main electron beam parameters (lattice v5.3).

Number of focusing & defocusing cavities	10 & 7	
RF Frequency, f_r	591.150	MHz
Quality Factor, Q	334364	
R/Q	37	
Voltage per Cavity, V_c	3.35	MV
Synchronous Phase, φ_s	179.05&0.95	deg
Detune Frequency (foc.)	-16240	Hz
Detune Frequency (def.)	16240	Hz
Total Cavity Voltage of foc. & def. cavities, $V_{c,tot,foc}$ / $V_{c,tot,def}$	33.52 & 23.47	MV
Total Generator Voltage of foc. & def. cavities, $V_{g,tot,foc}$ / $V_{g,tot,def}$	6.39 & 4.47	MV
Generator Phase of foc. & def. cavities, φ_g	158.1 & 21.9	

Table 2: RF system parameters.

13.1.2 Results from Mbtrack2 Code

By employing the parameter setup as presented in Table 3 for the 10 focusing cavities and 5 defocusing cavities, we can obtain the bunch length distribution, bunch longitudinal position, and energy spread along the bunch train with such reverse phase configuration [23–26]. Fig. 7

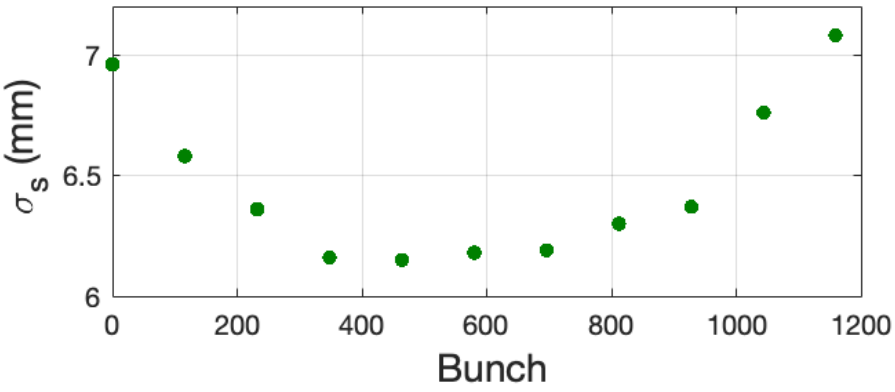

Fig. 4: The bunch length σ_s dependence on the bunch number M_i, $\sigma_s(M_i)$.

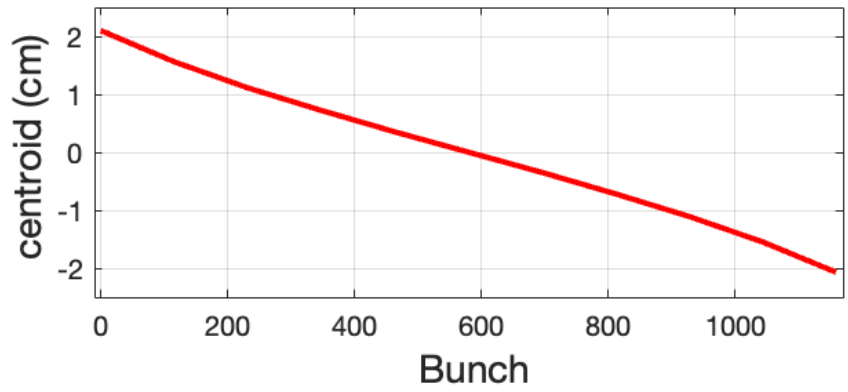

Fig. 5: Bunch centroid offset vs. the bunch number.

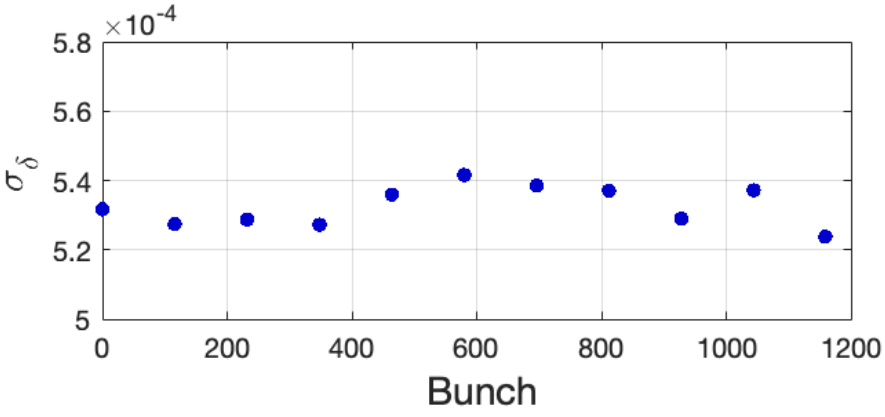

Fig. 6: The energy spread dependence on the bunch number M_i, $\sigma_\delta(M_i)$.

Table 3: 10F-5D reverse phase configuration RF parameters for mbtrack2

Parameter	**10 Focusing Cavity**	**5 Defocusing Cavity**
m	1	1
N_{cav}	10	5
Q	2e+10	2e+10
RoQ	37	37
$R_{s\_per\_cavity}$ [Ω]	7.4e+11	7.4e+11
R_s [Ω]	7.4e+12	3.7e+12
β	2.19784e+04	2.19784e+04
Q_L	9.09944e+05	9.09944e+05
R_L	33667928	33667928
$detune$ [Hz]	-1.63399e+04	1.63404e+04
f_c [Hz]	5.91134e+08	5.91167e+08
ω_c [rad/s]	3.71421e+09	3.71441e+09
ψ [deg]	-88.86	88.86
V_c [V]	3.35e+07	1.675e+07
θ_s [deg]	88.86	-88.86
V_g [V]	1.33158e+06	6.65788e+05
θ_g rad	1.80814e-06	-1.80829e-06
V_{gr} [V]	6.6997e+07	3.34985e+07
θ_{gr} [deg]	88.86	-88.86
V_b [V]	3.35e+07	1.675e+07
V_{br} [V]	1.68552e+09	8.42759e+08
P_g [W]	1.66657e+06	8.33285e+05
P_c [W]	7.58277e+01	3.79139e+01
P_b [W]	1.66649e+06	8.33247e+05
P_r [W]	2.51703e-10	9.43601e-12
n_{bin}	200	200
Filling time [s]	4.89980e-04	4.89953e-04
Loss factor [V/C]	6.87128e+11	3.43583e+11

presents the results of simulations with 290 bunches, 50k macro-particles, and 20k turns. The single cavity voltage is 3.35 MV, and the synchrotron phase is 88.86 degrees (178.86 degrees for cosine conversion).

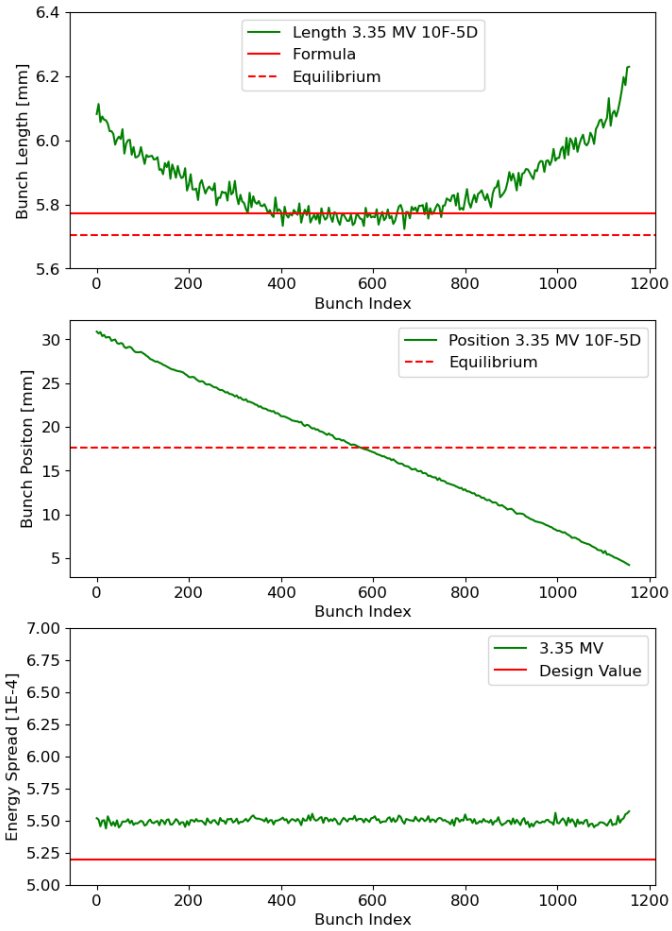

Fig. 7: The bunch length (top), bunch position (middle), and energy spread (bottom) depend on the index of the bunch within a bunch train.

The theoretical design values for bunch length and energy spread are indicated by the red solid lines in the figure. The bunch length is also evaluated using the equilibrium profile (represented by the red dashed line). The theoretical longitudinal bunch position for the two RF systems is calculated based on the equilibrium state formula. The energy spread is determined by the lattice itself.

The top plot of Fig. 7 shows that the bunch length exhibits an asymmetric parabolic shape for different bunch indices in a bunch train. The bunch length at the end of the bunch train is slightly larger than at the beginning. This result is consistent with the findings from the Elegant simulations above. The middle plot reveals that the centroid of the bunch train has a shift of 17.68 mm, displaying a linear distribution for the different bunches in the train. Additionally, the bunch energy spread is 5.5×10^{-4}, which is very close to the design value of 5.2×10^{-4}.

From these plots, we observe that the simulated bunch length, longitudinal bunch centroid,

and bunch energy spread closely match their theoretical values. Hence, we demonstrate that the mbtrack2 code accurately simulates these parameters, including the beam loading effect.

13.2 HSR Bunch Split Simulation with Beam Loading

The development of the Electron-Ion Collider (EIC) at Brookhaven National Laboratory aims to study high-energy collisions by colliding polarized electron and polarized hadron beams, which will be stored in an Electron Storage Ring (ESR) and a Hadron Storage Ring (HSR), respectively.

According to the EIC design parameters, the number of bunches in HSR at 275 GeV is 1160. Injection and acceleration will be performed with 290 bunches. At 275 GeV in storage mode, the bunches will be adiabatically split in two steps, from 290 bunches into 580 bunches, then again into 1160 bunches. As these two steps are similar, the paper focuses solely on the first step.

Bunch splitting involves manipulating radio frequency (RF) to alter the bunch structure, numbers, and intensity within a high-intensity synchrotron, serving as a particle collider's injector. Leveraging various harmonic RF systems, such as combining fundamental and higher harmonic RF systems, proves an efficient approach. Methods like two-fold and three-fold bunch splitting have been tested and effectively implemented at CERN PS. However, these implementations were tested without considering the beam-loading effect.

To simulate the beam loading effect caused by significant high beam intensity during the bunch splitting, the paper utilizes the mbtrack2 code. This code is used to validate and study potential issues related to beam loading during bunch splitting for the EIC project. In this paper, a Python code-named mbtrack2 is employed for this study.

13.2.1 Simulation Setup

The 275 GeV HSR bunch parameters are utilized for all the studies and are presented in Table 4.

Table 4: Bunch Parameters for Bunch Split Simulation

Parameters	Symbol	Value
Intensity	N_p	$6.9e^{10} * 4$
Bunch Length	σ_z[m]	0.75
Bunch Number	N_b	290
Energy	E [GeV]	275
Energy Spread	δ_p/p	$2.0e^{-4}$

Hadron bunches from the AGS will undergo an adapted RF capture and acceleration system—shifted from its RHIC operational frequency of 28MHz to 24.6MHz for the EIC. To optimize bunch train formation for maximum luminosity, a two-stage scheme will adiabatically split the hadron bunches into four bunches, requiring new normal conducting bunch splitting cavities at 49.3MHz and 98.5MHz, with two for each frequency.

For the EIC, 290 bunches will be injected, captured, and accelerated using an upgraded h=315, 24.6MHz RF system. Planned store scenarios involve 290, 580, or 1160 bunches, with the latter patterns produced through adiabatic splitting and subsequent compression.

To generate store patterns of 580 or 1160 bunches at h=630 or h=1260 respectively, new bunch splitting cavities at 49.3MHz (h=630) and 98.5MHz (h=1260) are necessary. Adiabatic bunch splitting, such as 1:2 or 1:2:4 splits, will generate these desired patterns. The cavity parameters used in the paper are presented in Table 5.

During simulation, we assume that the cavities could have a feedback system, and the Q for all cavities can be reduced to $\frac{1}{150}$ of their initial value.

Table 5: RF Cavity Parameters for Bunch Split Simulation

Cavity	**Parameters**	**Value**
$m = 1$	Q	14000
	Q_L	4700
	RoQ	42
	R_{sh} [kΩ]	584.2
	H	315
	Phase [degree]	180
	Voltage [MV]	0.4
	Frequency [MHz]	24.8
$m = 2$	Q	12200
	Q_L	3350
	RoQ	26.2
	R_{sh} [kΩ]	321
	H	630
	Phase [degree]	0
	Voltage [MV]	0.6
	Frequency [MHz]	49.2
$m = 3$	Q	9500
	Q_L	2780
	RoQ	28
	R_{sh} [kΩ]	267.2
	H	1260
	Phase [degree]	180
	Voltage [MV]	0.9
	Frequency [MHz]	98.6

For effective adiabaticity and preservation of the desired longitudinal emittance, the splitting time should typically span many synchrotron periods. However, our primary goal is to simulate the beam loading effects on the different longitudinal bunch positions along the bunch train (bunch index). To obtain rapid results, the splitting time is not extensively studied in this paper.

Figure 8 shows the voltage evaluation as a function of simulation turns during the 1:2 split simulation.

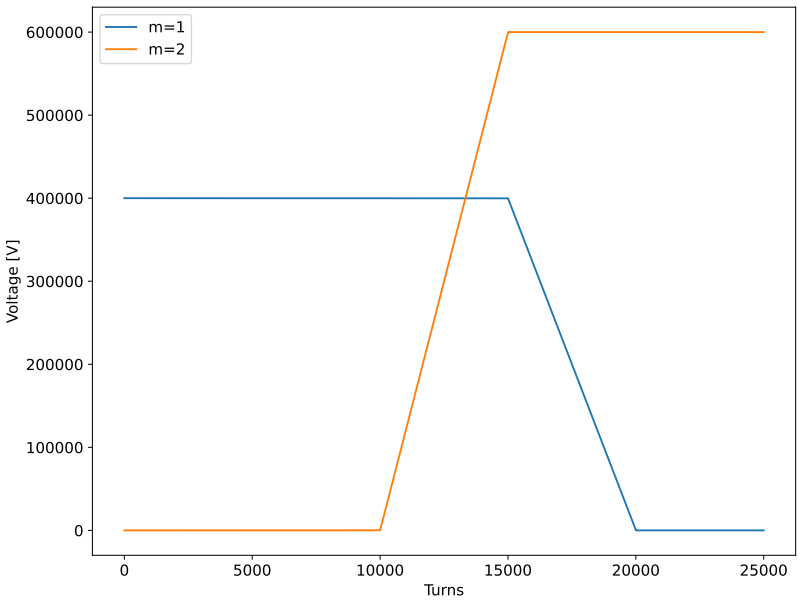

Fig. 8: Cavity Voltage as function of tracking turns.

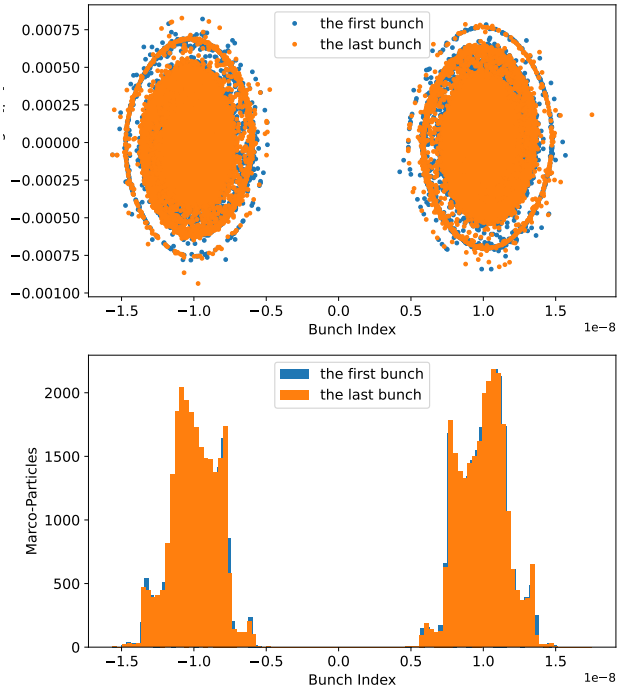

Fig. 9: Macro-particle distribution within the bunch after splitting in phase space (top plot) and in diagram (bottom plot)

13.2.2 Phase Space for the first and the last bunch

After simulation, one proton bunch is split into two bunches, as shown in Fig. 9. The top plot of the figure displays the phase space of the first (blue) and last (orange) bunches, while the bottom figure illustrates the macro-particle count for these two bunches after splitting. We observe that the proton bunches are split into the left and right bunches for the first and last bunches, respectively.

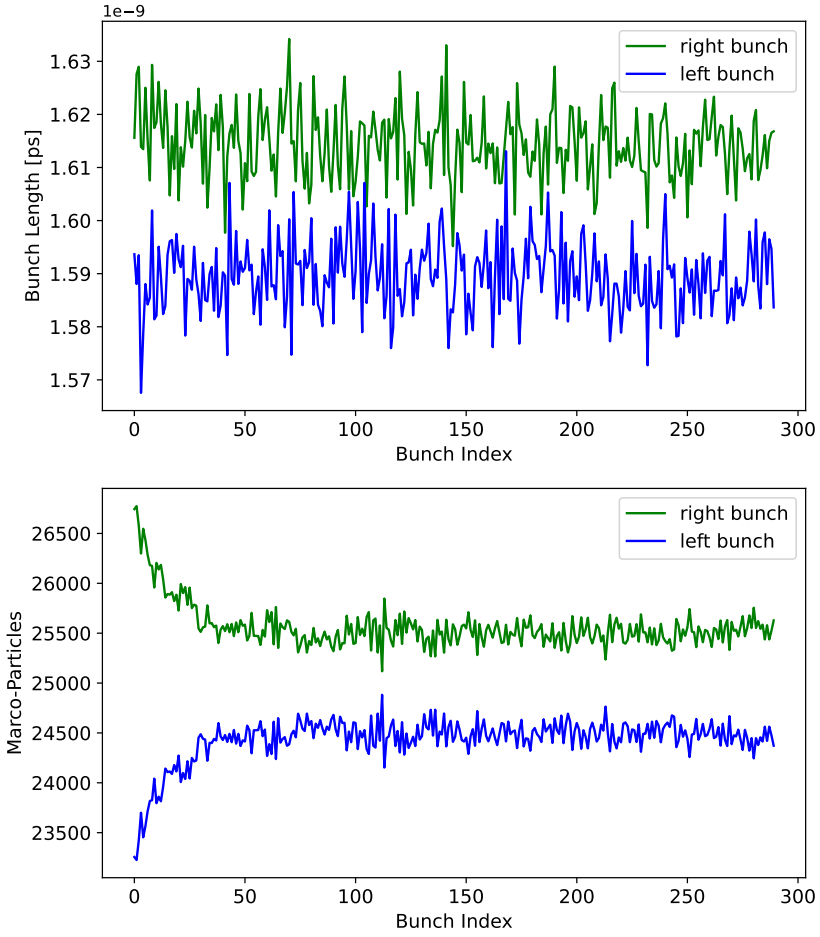

Fig. 10: Bunch Length and Macro-particle as function of tracking turns.

Referring to the top figure in Fig. 9, we can determine the bunch length and energy spread after splitting for the left and right bunches.

Examining the bottom figure in Fig. 9, we notice that after splitting, the number of macro-particles in the left and right bunches differs. The right bunches contain more macro-particles than the left bunches.

13.2.3 beam parameters along the bunch train

Fig. 10 depicts the bunch length and macro-particles for the left and right bunches following the splitting of 290 bunches. The X-axis represents the bunch index number.

In the upper figure of Fig. 10, we observe that the bunch lengths for the left and right bunches post-splitting are very close, showing no significant differences.

Examining the lower figure in Fig. 10, we note a disparity in the macro-particle bunch numbers between the left and right bunches (5100 vs. 4900), especially evident in the initial 50 bunches prior to the 290-bunch splitting.

Fig. 11 displays the bunch length and macro-particle ratio between the left and right bunches post-splitting. Both Fig. 10 and Fig. 11 indicate an uneven distribution of macro-particles between the left and right bunches after splitting. Particularly noticeable is the disparity in the first bunch (prior to splitting), where post-splitting, the right bunch measures approximately 0.15 higher than the left bunch.

To mitigate this uneven distribution of macro-particles, attributed from the beam loading effect, optimization has been pursued using both cavity voltage and phase adjustments for the fundamental cavity.

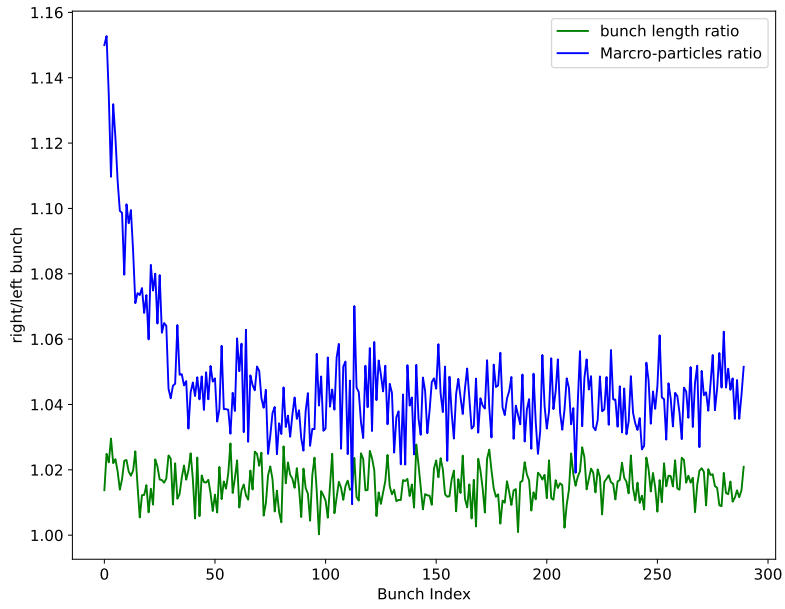

Fig. 11: Bunch Length and Macro-particle ratio (betweet right and left) as function of tracking turns.

14 Accelerator Specification Development for Instrumentation Hardware/Systems

14.1 Evaluation of Beam Position Monitors

The simulations were performed for evaluating signal levels from hadron and electron beams in different accelerators (hadron storage ring, electron storage ring, rapidly cycling synchrotron). The main goal of these simulations was to verify expected performance of beam position monitors (BPM). The signal level calculations were performed for the realistic beam parameters: for low end of dynamic range pilot bunch was used, and for the upper dynamic range full current with shortest bunch length was used. Figure 1 shows the simulations for the gold pilot bunch passing through a triplet BPM (122 mm diameter vacuum chamber).

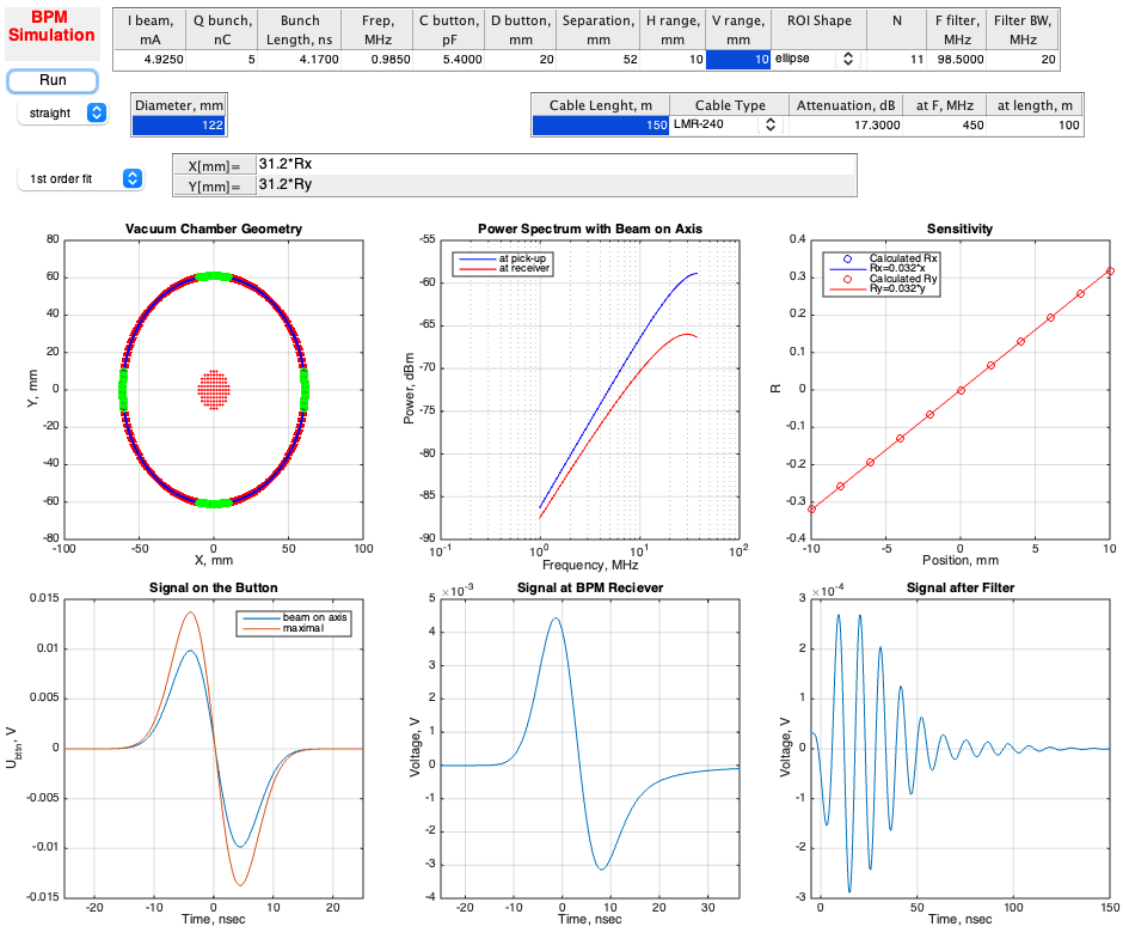

Fig. 12: Output of the MATLAB script for the gold pilot bunch inside the triplet BPM.

The simulation results are used for determination of the dynamic range of the BPM electronics, calculation of the scaling coefficient and polynomial fit for position calculations.

Substantial efforts were devoted for the corner BPM in the hadron ring since the procurement of

them will start this financial year. The analyses was done for the estimate of the button and BPM housing heating by the induced wake-fields for the strongly displaced hadron beam. More detailed report can be found in [27]. including impedance analyses, heating evaluation, and other engineering tasks. Another effort was done for reduction of the systematic errors due to the non-linear response of signal amplitude on beam position. The fifth order polynomial fit reduces the error to the acceptable level.

The precision of the measurement is defined by the signal-to-noise ratio. The following noise sources are being evaluated in the separate MATLAB script: thermal noise, external RFI noise, ADC clock jitter, effective number of bits for ADC.

14.2 Finding electrical Center of BPM

To maintain the polarization of the stored hadron beam, its trajectory should go through the arc quadrupole centers with high accuracy. Since the quadrupoles are fed in series it is impossible to perform beam-based alignment for individual quadrupole. BPMs will be installed with mechanical alignment relative to the quadrupole center, but we need to account for the electrical center of the quadrupole defined by unequal gains in the BPM channels. We are developing procedure for calibration of the channel gains with analyzing of the beam induced signal.

14.3 Diagnostics with synchrotron light

We are using SRW software for evaluation of a visible synchrotron radiation for the beam size measurement in the electron storage ring. Another application is to use streak-camera for measurement of the bunch length.

Using undulator radiation makes possible measurement of the beam energy, energy spread and beam emittance. Even for the hadron beam sufficient power can be generated to be observed. We can utilize existing CeC undulators with 4 cm period and 1.4 kGs peak field. The performance evaluation is under way.

15 Calculations of Electron Polarization in the ESR, RCS and HSR

Preliminary studies of polarization performance for the new RCS lattice have been started. Based on calculations of the intrinsic spin resonance strength in the RCS energy range, we observe that polarization transmission over the intrinsic spin resonances is still very good for new lattice. We can achieve over 90% transmission for 1000 mm-mrad normalized emittance through all intrinsic resonances using the standard 0.176 GeV/msec ramp rate. This polarization performance is better

than our previous RCS lattice. Some preliminary spin-orbit tracking appear to confirm these calculations. However we still need to complete analysis of the imperfection spin resonances for this new lattice, though we anticipate similar if not better results based on the intrinsic resonances strengths.

Polarization studies have been conducted using two codes: SITROS and Bmad. The polarization results, both with and without machine errors, demonstrated good agreement between the two codes. Studies using the SITROS code enabled the finalization of the BPM and dipole corrector configuration choice in the ESR [28]. A novel technique for minimizing depolarization, which involves specially selected knobs for vertical orbit bumps in the ESR arcs, has been proposed and thoroughly studied with the Bmad code [29]. This technique, named BAGEL, is designed to compensate for the longitudinal spin mismatch originating from spin rotators by minimizing the $dn/d\gamma$ function in the ring arcs. Remarkably, it can also be used to counteract depolarization caused by machine errors and can be employed for polarization tuning during operation. The studies showed that applying the BAGEL technique the equilibrium polarization can be significantly improved, ensuring the achievement of average polarization goal of 70%.

In the HSR, spin simulation studies with the code Zgoubi have continued, using an available HSR lattice with two interaction regions. Following a decision to include Low Energy Cooling into the EIC, simulation studies with different numbers of Snakes have been conducted. With the Low Energy Cooler, the proton and helium-3 beams are pre-cooled at the injection energy, reducing vertical emittance by nearly a factor of 10. This should help with polarization preservation during the acceleration ramp. However, the studies showed that the number of Snakes cannot be reduced: six Snakes are necessary to avoid polarization losses. Moreover, for the helium-3 beam, even with pre-cooled emittance and six Snakes, strong polarization losses are observed above 140 GeV/u. Calculations of the spin resonance strength for the HSR lattice showed that while the strongest resonances are decreased, as compared with the RHIC lattice, the resonance strength of most spin resonances is increased. This may explain the observed challenges in polarization preservation. To address the depolarization issues, studies have been initiated in two directions. One study looks at the possibility of adjusting the HSR lattice to reduce the spin resonance strength, which may result in additional quadrupole power supplies to make independent optics adjustments in different ring sextants. Another study aims at optimizing the orientation of the Snake spin rotation axes to improve the efficiency of spin resonance crossing.

In another development in the HSR, the spin rotator configuration has been verified with Zgoubi simulations [30]. The spin tune shift during the spin rotator turn-on process has been re-evaluated. It has been confirmed that the spin tune shift can be compensated by a moderate adjustment of the spin rotation axis in the Snakes.

16 Summary

Work supported by Brookhaven Science Associates, LLC under Contract No. DE-SC0012704 with the U.S. Department of Energy.

References

[1] C. Montag, *et al.*,, "Design Status of the Electron-Ion Collider", presentd at IPAC'23, VEnice, Italy, May 2023, paper MOPA049

[2] Bassi, G., Blednykh, A. and Smaluk, V. Self-consistent simulations and analysis of the coupled-bunch instability for arbitrary

[3] M. Borland, "elegant: A Flexible SDDS-Compliant Code for Accelerator Simulation," ANL/APS LS-287, 2000.

[4] https://gitlab.synchrotron-soleil.fr/PA/collective-effects/mbtrack2

[5] D. Marx *et al.,* "Designing the EIC Electron Storage Ring for Energies down to 5 GeV", presented at IPAC'23, Venice, Italy, May 2023, paper MOPA037

[6] Y. Nosochkov *et al.,* "Dynamic Aperture Studies for the EIC Electron Storage Ring", presented at IPAC'23, Venice, Italy, May 2023, paper MOPA048

[7] J. Unger *et al.,* "Interaction region effects on the EIC's Dynamic Aperture", presented at IPAC'23, Venice, Italy, May 2023, paper MOPA053

[8] H. Lovelace, III, F. Lin, C. Montag and V. Ranjbar, JACoW **IPAC2023** (2023), WEPL088 doi:10.18429/JACoW-IPAC2023-WEPL088

[9] V. Ranjbar, B. Lepore, H. Lovelace, III, M. Blaskiewicz, W. Xu, F. Meot, F. Lin and T. Satogata, JACoW **IPAC2023** (2023), MOPA035 doi:10.18429/JACoW-IPAC2023-MOPA035

[10] CST Particle Studio, http://www.cst.com

[11] W. Bruns, http://www.gdfidl.de

[12] I. Zagorodnov, "Indirect methods for wake potential inte- gration", Phys. Rev. ST Accel. Beams, vol. 9, p. 102002, 2006. doi:10.1103/PhysRevSTAB.9.102002

[13] H. Zhao, J. Kewisch, M. Blaskiewicz, and A. Fedotov, Phys. Rev. Accel. Beams 24, 043501 (2021)

[14] A. Blednykh, M. Blaskiewicz, R. Lindberg, D. Zhou, Phys. Rev. Accel. Beams 26, 051002 (2023)

[15] R. Li, M. Blaskiewicz, "IMPACT OF COHERENT BEAM-BEAM INTERACTION ON THE LANDAU DAMPING OF THE TRANSVERSE COUPLED-BUNCH INSTABILITY", IPAC2021 TUPAB258.

[16] M. Blaskiewicz "Instabilities driven by the fundamental crabbing mode" EIC-ADD-TN-023, October 2021.

[17] D. Boussard, Control of Cavities with High Beam Loading *IEEE Transactions on Nuclear Science*, **32**, #5, p.1852, 1985

[18] P. Baudreghien, T. Mastoridis, J. Molendijk, The LHC One-Turn Feedback, CERN-ATS-Note-2012-025 PERF, 2012

[19] M. Blaskiewicz "LANDAU DAMPING WITH HIGH FREQUENCY IMPEDANCE", PAC09 FR5RFP030.

[20] M. Blaskiewicz, NAPAC'2019, TUPLM11

[21] A. Chao "Physics of Collective Beam Instabilities in High Energy Accelerators", John Wiley and Sons, New York, 1993.

[22] Y. Morita et al., Proc. 14th Int. Workshop on SRF, Berlin, Germany, 236 (2009).

[23] doi:10.18429/JACoW-IPAC2021-MOPAB070, IPAC2021, Campinas, SP, Brazil

[24] X. Gu et al., EIC Tech Note: EIC-ADD-TN-066

[25] X. Gu et al., BNL-225173-2024-TECH, OSTI ID: 2281584

[26] Kevin S. Smith APEX Workshop, November 9, 2021 https://indico.bnl.gov/event/13401/

[27] F. Micolon, *et al.,*, "Thermal simulation of the HSR arc BPM Module for EIC", BNL Tech. Note BNL-224218-2023-TECH; EIC-ADD-TN-050. doi.org/10.2172/1969913

[28] SITROS studies were done by E. Gianfelice-Wendt (FNAL).

[29] BAGEL technique idea and studies have been done by M. Signorelli and G. Hoffstaatter 9Cornel University).

[30] K. Hock, *et al.,*, "An Overview of Helions in the HSR and its Injectors", submitted to Proceedings of SPIN'23 Symposium.